Journal of Solid State Chemistry 183 (2010) 1194–1199

Contents lists available at ScienceDirect

Journal of Solid State Chemistry

journal homepage: www.elsevier.com/locate/jssc

Investigation on the structural and electrical properties of $NdSrNi_{1-x}Cr_xO_{4+\delta}$ $(0.1 \leq x \leq 0.9)$ system

Manel Jammali, H. Chaker, K. Cherif, R. Ben Hassen *

Unité de Recherche de Chimie des Matériaux (02/UR/12-01), ISSBAT, Université de Tunis El Manar, 9 Avenue Dr. Zoheir Safi, 1006 Tunis, Tunisia

ARTICLE INFO

Article history:
Received 21 November 2009
Received in revised form
12 March 2010
Accepted 17 March 2010
Available online 25 March 2010

Keywords:
Sol–gel method
X-ray powder diffraction
LnSrNiCrO system
K_2NiF_4
Conductivity
Small polaron hopping model

ABSTRACT

The phases $NdSrNi_{1-x}Cr_xO_{4+\delta}$ $(0.1 \leq x \leq 0.9)$ have been synthesized by modified sol–gel method and subsequent annealing at 1250 °C in 1 atm of flowing argon. X-ray diffraction (XRD) analysis and electrical resistivity have been measured at room temperature. Rietveld refinement shows that all compositions with $x > 0.1$ were found to crystallize in the tetragonal K_2NiF_4 type structure in the space group $I4/mmm$, while for $x = 0.1$, a mixture of two phases with the tetragonal space group $I4/mmm$ and the orthorhombic space group $Fmmm$. Variations of a and c parameters show a complex behavior with increasing chromium content. It was established that compounds with chromium content less then $x \leq 0.5$ are oxygen-deficient, while for $x > 0.5$ the sample are oxygen-overstoichiometric. The $NdSrNi_{0.5}Cr_{0.5}O_{4+\delta}$ compound exhibits semiconductive behavior and the electrical transport mechanism agrees with the non-adiabatic small polaron hopping model in the temperature ranges 298–493, 493–573 and 573–703 K separately.

1. Introduction

The mixed ionic and electronic conducting oxides (MIEC) have attracted interest for use in a wide range of applications such as cathodes for solid oxide fuel cell (SOFC), electrodes for electrically driven ceramic oxygen generators (COG) or dense ceramic membranes for pressure driven oxygen separators [1] such as the mixed-conducting complex oxide $La_2NiO_{4+\delta}$ prepared by complex sol–gel method [2]. The $Ln_2NiO_{4+\delta}$ oxides can be good candidates for these types of applications because of the high level of their electronic and ionic conductivities. They are good electronic conductors due to the mixed (Ni^{+3}/Ni^{+2}) valence of the nickel cations [1]. Oxygen ionic conduction in K_2NiF_4-type compounds may occur via a vacancy mechanism in the perovskite layers and via diffusion of oxygen interstitials in the rock-salt-type layers [3]. On the other hand, many extensive investigations have been carried out on the structural, electrical and magnetic properties on the Sr-doped rare earth nickelates, in particular, the Ni^{II}/Ni^{III} $Nd_{2-x}Sr_xNiO_4$ [4,5,9,10] and $La_{2-x}Sr_xNiO_{4+\delta}$ compounds [6–8]. All the iodometric and thermogravimetric analysis results established on these series of compounds illustrated that samples with low strontium contents tend to accommodate excess oxygen, while those with high strontium contents are slightly oxygen deficient. Naturally this is to be expected, as the greater the value of x, the greater the proportion of Ni^{II} which must be oxidized to Ni^{III} in the sample in order to preserve overall charge neutrality if the oxygen stoichiometry is maintained [11].

It has also been reported in previous works that the $Ln_2(M,Ni)O$ and $LnSr(M,Ni)O_4$ systems (where M=Co, Fe, Cr, Cu) show complete miscibility both at room and at higher temperature [12–21]. The Goodenough [22] rules predict that if two cation species, B and B′, with appropriate electron configurations (for example d^3 and d^5 or d^5 and d^8) are present in an insulating oxide, then the superexchange interaction between them can be ferromagnetic, provided that the B–O–B′ bond angle is close to 180°. According to the model developed by Tan et al. [23], the degree of localization of the transition-metal d electrons depends on the overlap integrals with the neighboring transition-metal cation's d states. Moreover, the simultaneous presence of several transition elements in oxide diluted solid solutions usually results in rich properties, such as electrical and magnetic ones. In the study of $LaSrNi_{1-x}Cr_xO_{4+\delta}$ [16], synthesized under argon atmosphere, Millburn and Rosseinsky have well described the effect of Cr^{3+} substitution on the crystal structure, magnetism and chemical reactivity in $LaSrNiO_4$, as an important member of the $La_{2-x}Sr_xNiO_{4\pm\delta}$ solid solutions [24]. They showed that the samples with high chromium content are overstoichiometric in oxygen and the small amounts of excess oxygen may be attributed to the partial oxidation of Cr^{III} to Cr^{IV}.

In order to get more insight of the structural and electrical properties in this family of compounds, we have synthesized and characterized new solid solutions by substituting both strontium

* Corresponding author.
E-mail address: rached.benhassen@fss.rnu.tn (R. Ben Hassen).

0022-4596/$ - see front matter © 2010 Elsevier Inc. All rights reserved.
doi:10.1016/j.jssc.2010.03.028

and chromium into the parent compound Nd_2NiO_4. We describe below our attempts to synthesize this series of compounds, and the subsequent characterization of our reaction products by resistivity and X-ray diffraction techniques. Our results are compared with those obtained on related papers in the literature [16].

2. Material and methods

The solid solutions of the $NdSrNi_{1-x}Cr_xO_{4+\delta}$ system were prepared for all compositions $x=0.1$; 0.3; 0.5; 0.7 and 0.9 using sol–gel method, stoichiometric quantities of Nd_2O_3 (99.99%, Aldrich, calcined in air at 800 °C to remove adsorbed water and carbon dioxide), $SrCO_3$ (99.99%, Aldrich), NiO (99.99%, Aldrich) and $Cr(NO_3)_3 \cdot 9H_2O$ (99.99%, Aldrich), as appropriate, were dissolved in a minimum quantity, typically 150 ml, of a 1:1 solution of analar 6 M nitric acid and distilled water, Then, 5 ml of ethylene glycol (99.99%, Aldrich) and one equivalent of citric acid per mole of M^{3+} cation (99.99%, Aldrich) were added and the solution was heated at 150 °C on a hot plate with constant stirring for approximately 3 h. The pale green gel thus formed was decomposed by further heating at 300 °C for approximately 24 h. The resulting fine brown powder was ground, and then returned to the furnace in air at 800 °C for between 24 and 48 h. The obtained powder was pressed into 13 mm diameter at 10 ton. The pellets were annealed in a tube furnace at 1250 °C in 1 atm of flowing argon (dried by bubbling through concentrated sulfuric acid) for 6–8 days with several intermittent grindings. The black polycrystalline solid products were allowed to cool under the argon flow at the rate of the furnace, typically 12 h, before being removed.

The X-ray powder diffraction was carried out using the X'Pert Diffractometer operating with Cu $K\alpha_1/K\alpha_2$ radiation. Data were collected at each 0.0167° step width for 30 s over a 2θ range from 15° to 119°. Rietveld refinements of the crystal structure were performed using the FULLPROF program [25]. The line shape of the diffraction peaks was generated by a pseudo-Voigt function. The background was chosen by interpolation between selected points in regions devoid of Bragg reflections. In the final run the following parameters were refined: zero point, U, V, W, background points, pseudo-Voigt, scale factor, unit cell parameters, positional parameters, isotropic thermal factors and preferred orientation parameters.

The oxygen content of all the compositions system has been determined indirectly at room temperature after calculation of the valence average of the transition metal ions obtained by iodometric titration under flowing nitrogen gas taking into account that Ni^{3+} and Cr^{4+} can be present in the sample with Ni^{2+} and Cr^{3+}. In fact, about 100 mg of sample was dissolved in a solution of 6 M hydrochloric acid in the presence an excess of KI, leading to reduction of tri- and tetra-metal transition ions and formation of iodine that was titrated with $Na_2S_2O_3$ solution using starch as indicator. Sodium thiosulfate solution was standardized using pure copper wire [26].

The Electrical direct current resistivity measurements were carried out on sintered pellets using a Lucas Labs 302 four point probe with a Keithley 2400 digital. Source Meter (Keithley Instruments, Inc., Cleveland, Ohio). Measurements were performed at room temperature for all compositions. Impedance spectroscopy measurements of the sample with $x=0.5$ only, using a sintered polycrystalline disk form, have been carried out in the temperature range 298–682 K. Electrical contacts are made by silver paste. The spectroscopy analyser used is a HP analyser for solid state. The frequency range is from 100 Hz to 10 MHz. Impedance diagrams were analyzed and fitted using the Z view software [27]. The resistance R was derived from the low-frequency intersection of a semicircle fit on the complex impedance plane with the real complex axis. The conductivity was calculated using the following relation:

$$\sigma = d/RS[\Omega^{-1} \cdot m^{-1}]$$

3. Results and discussion

3.1. Structural study and oxygen stoichiometry analysis

The purity of the samples synthesized $NdSrNi_{1-x}Cr_xO_{4+\delta}$ ($0.1 \leqslant x \leqslant 0.9$) was confirmed by X-ray powder diffraction measurements, which revealed no product impurities or starting materials.

In order to study the variation in the oxygen stoichiometry as function of chromium content we have carried out iodometric titration using $Na_2S_2O_3$ standard solution. The oxygen nonstoichiometry (δ) is directly correlated to the Ni^{3+} and Cr^{4+} content according to the formulation $NdSr(Ni^{3+}_{1-\tau}\ Ni^{2+}_{\tau})_{1-x}(Cr^{4+}_{1-\tau}\ Cr^{3+}_{\tau})_xO_{4+\delta}$, with $\delta=(x-\tau)/2$. The content $(1-\tau)$ of the average of cations transition metals Ni^{3+} and Cr^{4+} was then determined by iodometric titration. I^- anions reduce Ni^{3+} cations into Ni^{2+} and Cr^{4+} cations into Cr^{3+}. The titration of the resulting I_2 by a solution of $Na_2S_2O_3$ sodium thiosulfate leads to determine (τ) and therefore (δ) whose values are reported in Table 1. The obtained results indicate that compounds with chromium content less then ($x \leq 0.5$) are oxygen-deficient, while for $x > 0.5$ the sample are oxygen-overstoichiometric.

The crystal structures of samples with $x > 0.1$ were refined, from powder X-ray data, in the $I4/mmm$ tetragonal space group; this is the same space group adopted by the parent compounds $NdSrNiO_4$ and $NdSrCrO_4$ [28,29]. The isotropic temperature factors for the oxygen sites could not be refined and so the values were fixed, at 0.02 Å^2, in the final refinements. The positional and thermal parameters obtained are shown in Table 2. We have chosen the X-ray diffraction profiles of the composition $NdSrNi_{0.5}Cr_{0.5}O_{4+\delta}$ to be displayed in Fig. 1. The X-ray pattern of the $x=0.1$ sample showed a shift of some Bragg reflections that was indicative of a unit cell of lower symmetry. Two distortions of the $I4/mmm$ K_2NiF_4 aristotype cell to orthorhombic symmetry are known, $Fmmm$ and $I\ mmm$, depending on which of the $\langle 1\,0\,0 \rangle$ and $\langle 1\,1\,0 \rangle$ sets of mirror planes and twofold axes are lost together with the fourfold axis when the symmetry is lowered. Inspection of the X-ray pattern indicates that the h 0 l reflections remain unsplit. Such an observation suggested refinement of the data in the $Fmmm$ space group with unit cell related to the tetragonal structure ($I4/mmm$) by $a_o \approx b_o \approx \sqrt{2}a_t$ and $c_o \approx c_t$. However, Rietveld refinement of the powder X-ray data for the $x=0.1$ sample in $Fmmm$ produced an unsatisfactory fit. Refinement was then attempted with a two-phase model, in which an undistorted $I4/mmm$ structure is introduced as a second phase. Such an attempt has been encountered in the study of

Table 1
Oxygen content and average transition metal oxidation state valence for all compositions.

Chromium content (x)	Oxygen content	Average transition metal oxidation state
0.1	3.85	2.70
0.3	3.95	2.90
0.5	3.98	2.96
0.7	4.02	3.04
0.9	4.03	3.06

chromate nickelate, LaSr $Ni_{0.9}Cr_{0.1}O_{3.75}$ [16]. The observed, calculated, and difference profiles for this refinement are shown in Fig. 2 with an enlargement of the fit to the 31.8–33.6° 2θ region. Similar multiphase refinements indicated that the orthorhombic phase was not present in any of the samples with higher values of x, nor did the data for these samples refine satisfactorily in any other related lower symmetry space groups. The observed, calculated and difference profiles parameters obtained are shown in Table 3. The difficulty in forming a single phase may be qualitatively attributable to the conflicting requirements of the different oxidation states which need to be stabilized. As the percentage chromium content, x, is decreased, i.e., as the percentage nickel content increased, the total oxygen content of the samples, and thus the average transition-metal oxidation state, decreases quite dramatically (Table 1); samples containing 50% nickel and 50% chromium are approximately stoichiometric: the small amounts of excess oxygen for $x > 0.5$ may be attributed to partial oxidation from Cr^{III} to Cr^{IV} ($\delta = 0.02/0.03$), whereas the sample with 90% nickel and 10% chromium contains only 3.85 oxygen per formula unit ($\delta = -0.15$). It is clear that the greater the proportion of nickel in the samples, the more difficult is the total formation of Ni^{III} from Ni^{II} under the synthesis conditions. The smaller deviations in the oxygen stoichiometry from 4.02 for the sample with $x > 0.5$ indicates exclusive formation of Ni^{III}, which is at first sight surprising given that the phases can be prepared only under argon. Increasing the concentrations of chromium cosubstituted on the octahedral site clearly enhances the stability of Ni^{III}. This may be explained in terms of the less electronegative nature of Cr^{III} compared with Ni^{III}. Competition for donation from the oxide anion to a Ni^{III} center is reduced as the Cr^{III} concentration increases; the Cr^{III}–O bond is more ionic, and thus Ni^{III} is stabilized via increased covalency with oxide anion. At lower Cr^{III} concentrations ($x = 0.1$), the Ni^{III} oxidation state is not stable under these reaction conditions and oxygen vacancies form under the argon synthesis atmosphere. The tendency of these vacancies to order crystallographically results in the *Fmmm* structure forming in competition with the disordered *I*4/*mmm* structure in a two-phase sample. Such observations have been encountered in the study of the system $LaSrNi_{1-x}Cr_x\ O_{4+\delta}$ [16].

Table 2
Structural parameters of $NdSrCr_xNi_{1-x}O_{4\pm\delta}$ obtained from Rietveld refinements of powder X-ray diffraction data[a].

x		0.3	0.5	0.7	0.9
a (Å)		3.79318(4)	3.80347(4)	3.82236(2)	3.83371(2)
c (Å)		12.4581(2)	12.4755(2)	12.3977(1)	12.3548(1)
c/a		3.2846	3.2800	3.2435	3.2227
V (Å^3)		179.262(4)	180.475(3)	181.136(2)	181.582(2)
Nd/Sr	z	0.35955(8)	0.35877(7)	0.35924(7)	0.35926(6)
	U_{iso} (Å^2)	0.0158(3)	0.0156(3)	0.0198(3)	0.0211(3)
Cr/Ni	U_{iso} (Å^2)	0.0163(7)	0.0173(6)	0.0187(7)	0.0185(7)
$O_{(1)}$	z	0.1659(5)	0.1661(5)	0.1663(5)	0.1649(5)
	U_{iso} (Å^2)	0.02	0.02	0.02	0.02
$O_{(2)}$	U_{iso} (Å^2)	0.02	0.02	0.02	0.02
R_{wp} (%)		16.1	14.2	17.1	15.7
R_p (%)		21.2	21.1	22.3	21.9
R_B (%)		4.37	4.31	4.91	3.9
R_F (%)		3.07	3.08	3.09	3.24
χ^2		3.45	2.05	4.33	3.17

[a] Thermal parameters were fixed in some cases as described in the text, the atoms were refined in the following Wyckoff positions of space group No, 139, *I*4/*mmm*

4(Nd/Sr) and 4O(1)	in (*e*)	(4*mm*)	(0,0,*z*)
2(Ni/Cr)	in (*a*)	(4/*mmm*)	(0, 0, 0)
4 O(2)	in (*c*)	(*mmm*)	(0,1/2,0)

The evolution of the cell parameters with the chromium content x (Table 2), shows the presence of a change in behavior both for a and c. The major one occurs with the c parameter, which increases, with increasing chromium content, from 12.4033(6) to 12.4755(2) Å up to $x = 0.5$, whereas the a parameter remains almost constant in this range. These trends in the cell parameters can be attributed to the Jahn–Teller distortions of the MO_6 octahedra (change in the e_g^1 configuration; d_z^2 orbital is occupied instead of the $dx^2 - y^2$). Table 4 shows variations of the axial and equatorial Ni/Cr–O bonds lengths versus x. For low x ($x < 0.5$), the samples are highly oxygen deficient, due to the presence of nickel atoms in mixed valence Ni^{III}/Ni^{II}. The small amounts of excess oxygen for $NdSrNi_{1-x}Cr_xO_{4+\delta}$ ($x > 0.5$) may be attributed to the partial oxidation of Cr^{III} to Cr^{IV}. Based on

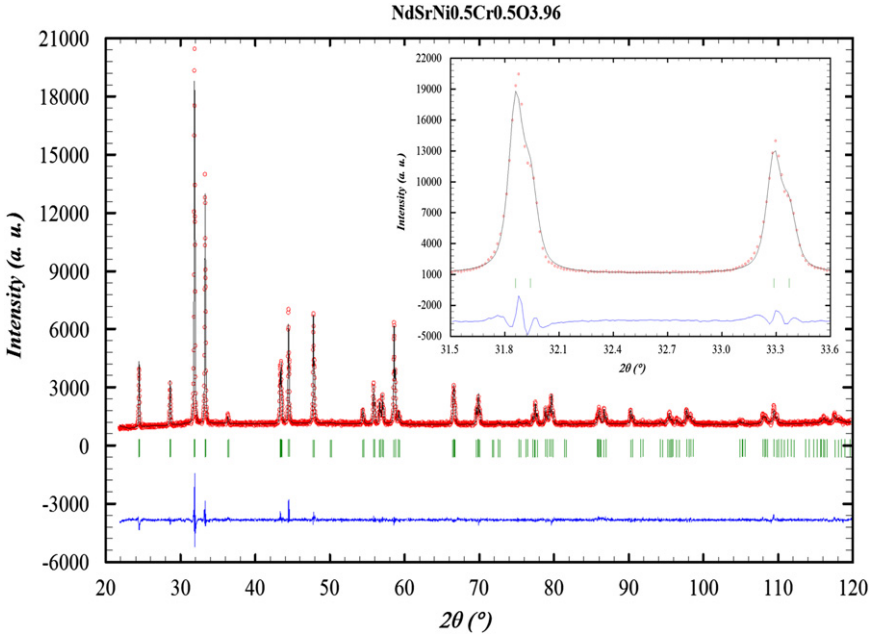

Fig. 1. Observed (markers), calculated (line), and difference profiles for the X-ray Rietveld refinements of $NdSrCr_{0.5}Ni_{0.5}O_{4+\delta}$ in the *I*4/*mmm* space group.

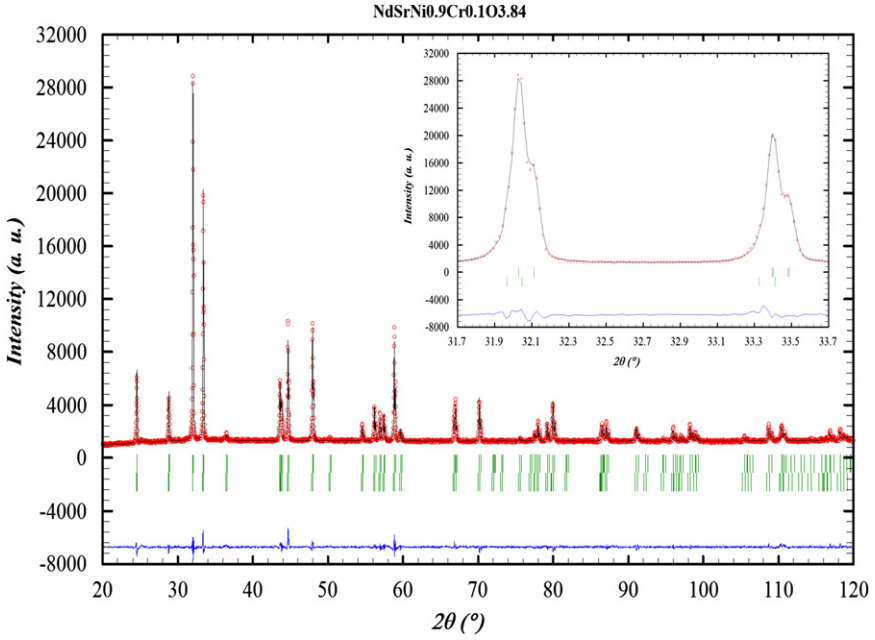

Fig. 2. Observed (crosses), calculated (continuous line) and difference. X-ray diffraction patterns for $NdSrCr_{0.1}Ni_{0.9}O_{4+\delta}$ with one *Fmmm* (75.52%) and one *I4/mmm* (24.48%) phases.

Table 3
Structural parameters obtained from multiphase Rietveld refinements of powder X-ray diffraction data for $NdSrCr_{0.1}Ni_{0.9}O_{4+\delta}$[a].

		Fmmm	I4/*mmm*
a (Å)		5.3620(9)	3.7993(1)
b (Å)		5.3606(9)	3.7993(1)
c (Å)		12.3830(1)	12.4033(6)
V (Å^3)		355.93(9)	179.03(1)
Fraction (%)		75.52	24.48
Nd/Sr	*z*	0.36023(7)	0.3592(3)
	U_{iso} (Å^2)	0.0066(2)	0.00507
Cr/Ni	U_{iso} (Å^2)	0.0096(6)	0.00507
$O_{(1)}$	*z*	0.1647(6)	0.181(2)
	U_{iso} (Å^2)	0.02	0.02
$O_{(2)}$		0.02	0.02

[a] Thermal parameters were fixed in the case of the *I4/mmm* phase and for the oxygen sites in *Fmmm* phase. The atoms were refined in the following Wyckoff positions of space groups No, 139, *I4/mmm* and No: 69, *Fmmm*.

4(Nd/Sr) and 4O(1)	in (*e*)	(4*mm*)	(0, 0, *z*)
2(Ni/Cr)	in (*a*)	(4/*mmm*)	(0, 0, 0)
4 O(2)	in (*c*)	(*mmm*)	(0, 1/2, 0)
8(Nd/Sr) and 8O(1)	in (*i*)	(*mm*)	(0, 0, *z*)
4(Ni/Cr)	in (*a*)	(*mmm*)	(0, 0, 0)
8 O(2)	in (*e*)	(2/*m*)	(1/4, 1/4, 0)

Table 4
Selected bond lengths (Å).

Chromuim content *x*	*x*=0.1	*x*=0.3	*x*=0.5	*x*=0.7	*x*=0.9
Ni/Cr–O(equatorial) Å	1.8996(1)	1.8966(2)	1.9017(3)	1.9112(1)	1.9169(3)
Ni/Cr–O(axial) Å	2.2435(2)	2.065(7)	2.073(7)	2.062(7)	2.038(7)

Shannon's ionic radii [30], we noted that Cr^{IV} ion (R_I=0.55 Å in six coordination) is smaller than Cr^{III} (R_I=0.615 Å in six coordination). For this reason, the parameter *c* decreases for the compositions corresponding to a higher percentage of chromium than nickel, the unit cell volume increases dramatically with *x* in the series $NdSrNi_{1-x}Cr_xO_4$, but the growth rate appears to decline for $x>0.5$ series. Qualitatively such an increase may be expected, assuming an ionic model, according to the larger effective ionic radius of six-coordinate Cr^{III} (0.615 Å) compared to that of Ni^{III}, whether high (R_{II}=0.60 Å ($t_{2g}^5e_g^2$)) or low spin (R_I=0.56 Å ($t_{2g}^6e_g^1$)) in an oxide environment [31]. Accordingly we noted the increase in *a* parameter for compositions $x>0.5$ in $NdSrNi_{1-x}Cr_xO_{4+\delta}$ system. This behavior was previously seen in the study of $LaSrCr_xNi_{1-x}O_{4+\delta}$ system and also reported for $La_{2-x}Ba_xNiO_4$ [32].

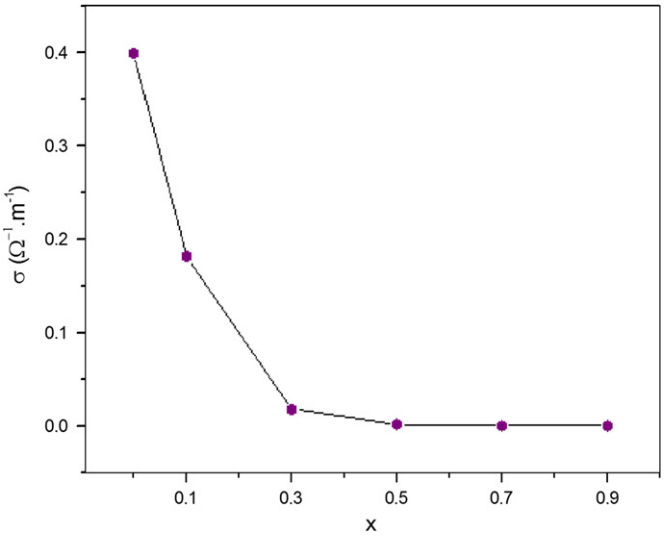

Fig. 3. Room temperature electrical conductivity as a function of chromium content in $NdSrNi_{1-x}Cr_xO_{4+\delta}$.

3.2. Electrical properties

The room temperature conductivity (σ_{RT}) values as a function of chromium content *x* are presented in Fig. 3. As can be seen, the

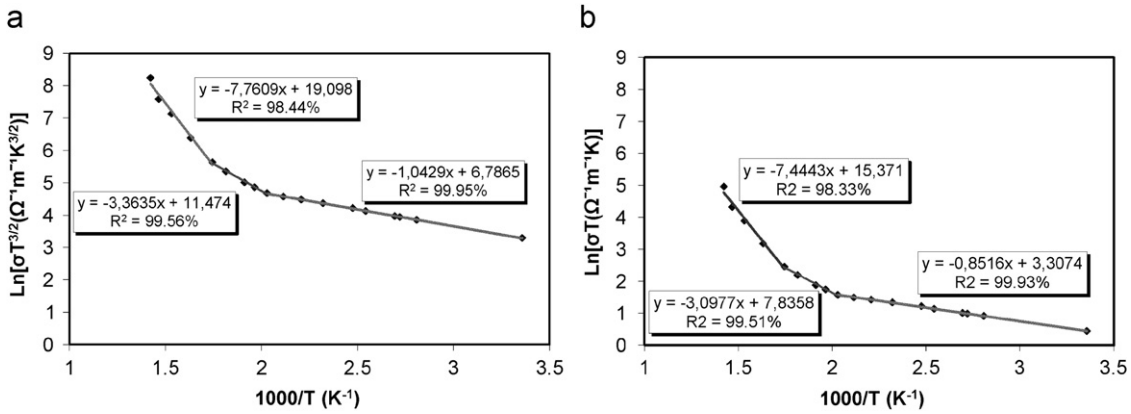

Fig. 4. (a) Arrhenius relations of $\mathrm{Ln}(\sigma T^{3/2})$ vs $1000/T$, (b) Arrhenius relations of $\mathrm{Ln}(\sigma T)$ vs $1000/T$ for the $NdSrCr_{0.5}Ni_{0.5}O_{4+\delta}$.

room temperature conductivity decreases rapidly up to $x=0.5$, then remains constant with increasing x. This observation correlates well with changes in the average valences of transition metal cations (Table 1), as a function of x, demonstrating the influence of mixed valent nickel and chromium on the room temperature properties. It is worth noting that the room temperature conductivity displays a decrease with increasing x, which is not parallel with the changes in the cell parameters. This behavior contrasts with the observations for the series $Nd(Cr_{1-x}Fe_x)O_3$ [33,35] where the room temperature conductivity is shown to follow the same trends as the cell parameter changes. In the polycrystalline samples the room temperature conductivity is expected to vary with the size and shape of the grain boundaries and hence precise estimation of the σ_{RT} values is often complicated, thus data on single crystals would be of help in resolving the differences between the Cr substituted Fe and Cr nickelates systems.

It was mentioned in literature [34,36,37] that $Ln(Ca,Sr)CrO_4$ are p-type semiconductors and exhibit hopping conductivity in a small-polaron model above room temperature. In our work, only $NdSrNi_{0.5}Cr_{0.5}O_{4+\delta}$ was chosen for the conductivity study at high temperatures. Measurements of conductivity versus temperature are shown in Fig. 4. The increase of $\mathrm{Ln}(\sigma T)$ with increasing temperature indicates that sample has semiconductor-like behavior. To determine the conduction mechanism; we use the thermal activated small polaron hopping as conduction model [23,38–40]

$$\sigma = \sigma_0 T^{-\alpha} \exp\left(\frac{-E_a}{k_B T}\right)$$

with E_a is the activation energy (polaron formation and hopping energy), σ_0 is a constant related to polaron concentration and diffusion. In the Arrhenius equation above, $\alpha=1$ corresponds to adiabatic small polaron hopping and $\alpha=1.5$ in the case of non-adiabatic small polaron hopping. In the analysis of simulated curves: $\mathrm{Ln}(\sigma T^{\alpha})=f(1000/T)$, we found that convergence of curve fitting is not achieved in the whole temperature range, but in areas of temperature (298–493, 493–573 and 573–703 K), and the best fitting is observed for a value of $\alpha=1.5$ in all three areas. This suggests that the charge transport in $NdSrNi_{0.5}Cr_{0.5}O_{4+\delta}$ ceramic always remains described by non-adiabatic small polaron hopping model, but with different activation energies in the regions of temperatures indicated above. Figs. 4a and b show the relationship of $\mathrm{Ln}(\sigma T^{3/2})$ and $\mathrm{Ln}(\sigma T)$ versus $10^3/T$ for temperature ranges 298–493, 493–573 and 573–703 K, respectively. The fitting parameters σ_0 and E_a are $\sigma_{0(1)}=8.86\,\Omega^{-1}\,m^{-1}$ and $E_{a(1)}=0.09$ eV, respectively, for temperature range 298–493 K, $\sigma_{0(2)}=961.82\,\Omega^{-1}\,m^{-1}$ and $E_{a(2)}=0.29$ eV for temperature range 493–572 K and $\sigma_{0(3)}=19.68\times10^5\,\Omega^{-1}\,m^{-1}$ and $E_{a(3)}=0.67$ eV for temperature range 572–703 K.

4. Conclusions

Chromium can be successfully substituted in place of nickel in the parent compound $NdSrNiO_4$, Rietveld refinements using powder X-ray diffraction data show that compounds in the solid solution $NdSrNi_{1-x}Cr_xO_{4\pm\delta}$ ($x>0.1$) crystallize with the tetragonal K_2NiF_4-type structure in space group $I4/mmm$, while for $x=0.1$, the sample was multiphasic due to the competition between the $Fmmm$ and the undistorted K_2NiF_4 structure. The a and c unit cell parameters values displayed variations with increasing chromium content, suggested from the presence of the mixed valence of the Ni^{2+}/Ni^{3+} and Cr^{3+}/Cr^{4+} ions. The transport mechanism in $NdSrNi_{0.5}Cr_{0.5}O_{4+\delta}$ has been investigated. The fitting shows that the non-adiabatic small polaron hopping model describes the experimental data better than the adiabatic small polaron hopping model.

Acknowledgment

The authors gratefully acknowledge the ICDD for financial support (Grant number: 09-04).

References

[1] F. Mauvy, C. Lalanne, J.M. Bassat, J.C. Grenier, H. Zhao, P. Dordor, Ph. Stevens, Journal of the European Ceramic Society 25 (2005) 2669–2672.
[2] L. Cheng, H. Tanghua, H. Zhang, Y. Chen, J. Jiang, Y. Nanru, Journal of Membrane Science 226 (2003) 1–7.
[3] E.J. Opila, H.L. Tuller, B.J. Wuensch, J. Maier, Journal of American Ceramic Society 76 (1993) 2363–2369.
[4] T. Nakamura, K. Yashiro, K. Sato, J. Mizusaki, Solid State Ionics 180 (2009) 1406–1413.
[5] M. Zaghrioui, F. Giovannelli, S. Pruvost, N. Poirot, I. Monot-Laffez, Journal of Magnetism and Magnetic Materials 305 (2006) 71–75.
[6] L. Goux, M. Gervais, F. Gervais, C. Champeaux, A. Catherinot, Applied Surface Science 252 (2006) 3085–3091.
[7] J. Gopalakrishnan, G. Colsmann, B. Reutert, Journal of Solid State Chemistry 22 (1977) 145–149.
[8] G. Demazeau, J.L. Marty, B. Buffat, J.M. Dance, M. Pouchard, P. Dordor B. Chevalier, Materials Research Bulletin 17 (1982) 37–45.
[9] B.W. Arbuckle, K.V. Ramanujachary, Z. Zhang, M. Greenblatt, Journal of Solid State Chemistry 88 (1990) 278–290.
[10] J.E. Greendan, G. Liu, B.W. Arbuckle, K.V. Ramanujachary, M. Greenblatt, Journal of Solid State Chemistry 97 (1992) 419–426.
[11] J.E. Millburn, M.A. Green, D.A. Neumann, M.J. Rosseinsky, Journal of Solid State Chemistry 145 (1999) 401–420.

[12] H. Chaker, T. Roisnel, M. Potel, R. Ben Hassen, Journal of Solid State Chemistry 177 (2004) 4067–4072.
[13] H. Chaker, T. Roisnel, O. Cador, M. Amami, R. Ben Hassen, Solid State Sciences 8 (2006) 142–148.
[14] H. Chaker, T. Roisnel, M. Ceretti, R. Ben Hassen, Journal of Alloys and Compounds 431 (2007) 16–22.
[15] F. Zhao, X. Wang, Z. Wang, R. Peng, C. Xia, Solid State Ionics 179 (2008) 1450–1453.
[16] J.E. Millburn, M.J. Rosseinsky, Chemistry of Materials 9 (1997) 511–522.
[17] J.A. Kilner, C.K.M. Shaw, Solid State Ionics 154–155 (2002) 523–527.
[18] V.V. Kharton, A.P. Viskup, A.V. Kovalevsky, E.N. Naumovich, F.M.B. Marques, Solid State Ionics 143 (2001) 337–353.
[19] V.V. Kharton, A.A. Yaremchenko, A.L. Shaula, M.V. Patrakeev, E.N. Naumovich, D.I. Logvinovich, J.R. Frade, F.M.B. Marquesa, Journal of Solid State Chemistry 177 (2004) 26–37.
[20] S. Miyoshi, T. Furuno, H. Matsumoto, T. Ishihara, Solid State Ionics 177 (2006) 2269–2273.
[21] S.E. Dutton, M. Bahout, P.D. Battle, F. Tonus, V. Demange, Journal of Solid State Chemistry 181 (2008) 2217–2226.
[22] J.B. Goodenough, Magnetism and the Chemical Bond, Wiley, New York, 1963.
[23] X.Y. Tan, C.L. Chen, K.X. Jin, S.G. Zhao, B.C. Luo, Physica B 403 (2008) 4050–4052.
[24] I. Gopalakrishan, G. Colsmann, B. Reutert, Journal of Solid State Chemistry 22 (1977) 145–149.
[25] T. Roisnel, J. Rodriguer-Carvajal, Materials Science Forum 378–381 (2001) 118–123.
[26] R.A. Day, A.L. Underwood, Quantitative Analysis, 6th Ed, Pearson/Prentice Hall, 1991.
[27] ZPlot for Windows Version 2.1.Scribber Associates Inc., 1999.
[28] Y. Takeda, M. Nishijima, N. Imanishi, R. Kanno, O. Yamamoto, M. Takano, Journal of Solid State Chemistry 96 (1992) 72–83.
[29] K. Sander, U. Lehmann, Hk. Müller-Buschbaum, Zeitschrift Für Anorganische und Allgemeine Chemie 480 (1981) 153–156.
[30] R.D. Shannon, Acta Crystallographica A 32 (1976) 751–767.
[31] S.C. Chen, K.V. Ramanujachary, M.M. Greenblatt, Journal of Solid State Chemistry 105 (1993) 444–457.
[32] J.A. Alonso, J. Amador, E. Gutiérrez-Puebla, M.A. Monge, I. Rasines, C. Ruíz-Valero, Solid State Communications 76 (1990) 1327–1331.
[33] F. Jin, T. Endo, H. Takizawa; M. Shimada, Journal of Solid State Chemistry (1994) 138–144.
[34] H.E. Höfer, W.F. Kock, Journal of Electrochemical Society (1993) 2889–2894.
[35] H. Taguchi, Journal of Solid State Chemistry (1997) 108–114.
[36] H. Taguchi, K. Hirata, H. Kido, Y. Takeda, M. Kato, K. Hirota, Solid State Sciences 11 (2009) 1222–1225.
[37] I. Zvereva, L. Zueva, F. Archaimbault, M. Crespin, J. Choisnet, J. Lecomte, Materials Chemistry and Physics 48 (1997) 103–110.
[38] A.R. Long, in: M. Pollak, B. Shklovskii (Eds.), Hopping Transport in Solids, North-Holland, Amsterdam, 1991, p. 207.
[39] N.F. Mott, E.A. Davis, Electronic Processes in Non-Crystalline Materials, Clarendon Press, Oxford, 1971.
[40] E. Iguchi, H. Nakatsugawa, K. Futakuchi, Journal of Solid State Chemistry 139 (1998) 176–184.